International Core Journal of Engineering Volume 12 Issue 6, 2026
ISSN: 2414-1895 DOI: 10.6919/ICJE.202606_12(6).0010

Simulation Analysis of Axle Load Transfer During Actual Traction and Braking

Ting Tang[1], Xiaoyang Liu[2], and Shuangxi Chen[3,*]

[1] School of Mechanical Engineering, Chengdu University, Chengdu 610106, China

[2] School of Mechanical Engineering, Chengdu University, Chengdu 610106, China

[3] School of Mechanical Engineering, Chengdu University, Chengdu 610106, China

Abstract

Driven by the Belt and Road Initiative, the demand for efficient transport has promoted the development of multimodal transport, particularly road-rail intermodal transport, to overcome the drawbacks of traditional railway freight. This paper investigates the axle load transfer problem of a specific type of road-rail combined vehicle during operation. Unlike existing studies that mostly employ idealized or simplified traction/braking conditions, this study innovatively introduces real traction and braking curves into the dynamic model, thereby accurately reproducing the actual operating conditions of the train. Through simulating various empty and loaded vehicle marshalling conditions, the axle load transfer characteristics under different train formations are systematically analyzed. On the basis of exploring the fundamental mechanisms inducing axle load transfer, three targeted improvement schemes are put forward. Numerical simulations are carried out for these schemes and compared with the original design, so as to obtain the quantitative values and variation laws of axle load transfer under different conditions. The findings can provide important theoretical data and engineering references for the structural design, performance optimization and manufacturing of road-rail combined vehicles.

Keywords

Road–rail Vehicle; Actual Traction Braking; Axle Load Transfer; Coupler Buffer Device.

1. Introduction

Railway transportation constitutes a critical pillar of China's economic development. However, traditional rail transport suffers from inherent drawbacks including low handling efficiency and limited transport diversity. Road-rail intermodal transport has emerged as one of the pivotal strategies to enhance operational efficiency and cut logistics costs [1].Since the 1930s, foreign countries have conducted research and application on road-rail dual-purpose vehicles, among which the representatives include the U.S.-based RailRunner [2-3], Unimog [4-5], Italy's Zephir800NC tractor, American LEAF, Viking-type rail-road hybrid vehicles, and Japan's DMV rail-road hybrid buses [6].China's research on road-rail dual-purpose vehicles started relatively late. In 1964, the NJ230 automobile was converted into a road-rail vehicle, and a series of such vehicles for engineering and transportation have been subsequently developed, including emergency rescue vehicles, aerial work platforms, TGC-series transport vehicles, and concrete mixer trucks [7-8].

Research on rail-road hybrid vehicles continues to advance, yet challenges like axle load transfer in conventional rail systems persist as key obstacles. This phenomenon of load redistribution among different wheelsets, caused by longitudinal forces (e.g., traction and braking forces) or centrifugal effects during curve negotiation, falls within the scope of longitudinal dynamics. Over the years,

ISSN: 2414-1895 DOI: 10.6919/ICJE.202606_12(6).0010

extensive studies have been conducted on the longitudinal dynamics of railway trains to address axle load transfer problems.Wang et al. [9] developed a fully nonlinear locomotive system stability model integrating the locomotive system and traction rod coupler. Using Poincaré sections with a composite bifurcation method that progressively adjusts forward speed, they demonstrated the significant impact of longitudinal motion on locomotive stability. Sun et al. [10] proposed an improved buffer model with damping and friction characteristics and simplified the air brake system for longitudinal impulse analysis of heavy-haul trains. Schwarz et al. [11] proposed a signal-based observability measurement method, offering computational advantages for nonlinear systems while maintaining flexibility in signal characteristics. Camil Craciun et al. [12] investigated variations in longitudinal force distribution under different operational resistance conditions. Wu et al. [13] incorporated wheel-rail adhesion control into longitudinal train dynamic simulations; results showed that adhesion control remarkably altered maximum traction, average speed, and internal forces, and parallel computing reduced time cost by nearly 46%. Magelli [14] integrated train longitudinal dynamics into multibody codes using virtual user force elements, improving computational efficiency by up to four times. Regarding axle load transfer, Wu et al. [15] derived equations for axle load transfer and ideal traction height of A-1-A axle-type locomotives, analyzing parameter impacts on adhesion efficiency through single-variable methods. Yang [16] noted that axle load transfer deteriorates significantly on gradients, governed mainly by slope angle rather than traction force. Liu [17] conducted theoretical and simulation studies on axle load transfer, established a SIMPACK-MATLAB co-simulation model for locomotive axle load transfer analysis. Wang et al. [18] developed a three-dimensional dynamic model for a specific HX heavy-haul electric locomotive based on rigid-body multibody dynamics theory. They derived analytical formulas for axle load transfer in this type of locomotive with symmetrically arranged axle-hugging traction systems, obtaining quasi-static axle load transfer results through computational analysis. Luo [19] established theoretical calculation formulas for axle load transfer in maglev trains, achieving similar results under quasi-static conditions. Subsequent research revealed that higher traction point elevations reduce adhesion efficiency, with this trend becoming more pronounced when the traction point exceeds coupler height. Xuan [20] proposed a novel acceleration/deceleration estimation method for vehicles by considering load transfer between front and rear wheels, utilizing at least two cascaded micro-load measurement devices on the track. Wei [21] developed a longitudinal-vertical dynamic model for a specific high-speed train type, investigating axle load transfer phenomena. Zhang [22] introduced a linear monorail model to examine how nonlinear time-varying harmonic dynamic axle loads observed in automotive-trailer road tests affect system stability.

Couplers are key components used to realize coupling, transmit longitudinal forces and provide buffering between railway vehicles, or between locomotives and vehicles. They exert a significant influence on the safety and stability of train operation, as well as on most longitudinal mechanical indicators. Wu et al. [23] found that derailment accidents predominantly occur due to locomotive derailment. Their analysis of two typical locomotive derailment incidents on tangent tracks demonstrated that couplers play a crucial role in preventing derailment. In the automatic coupling device of automated passenger rapid transit systems, certain mechanisms require appropriate slack to facilitate proper coupling. Om Prakash Yadav et al. [24] developed a simplified two-degree-of-freedom coupling mechanism model incorporating impact and friction actions, studying how coupler slack affects the longitudinal dynamics of rail vehicles. The research revealed that intermittent impacts and slack lead to significant adhesive sliding, causing abrupt acceleration changes and substantial vibration—particularly at higher excitation frequencies. This increases derailment risks. Zhang et al. [25] established a finite element model simulating intermediate couplers 'buckling behavior, investigating their bending resistance and buckling instability characteristics. The findings indicate that the proposed coupling modeling method better simulates energy absorption characteristics and unstable behaviors. Yang et al. [26] proposed a computational method for determining the maximum vertical sway angle of railway couplers, addressing limitations in conventional approaches. Based on dynamic models of faulty vehicles, they developed a novel

ISSN: 2414-1895 DOI: 10.6919/ICJE.202606_12(6).0010

calculation framework. Hu[27] conducted field experiments to analyze operational conditions of coupler-worn trains. The study then systematically investigated theoretical causes of abnormal wear through structural analysis, ultimately proposing countermeasures to mitigate excessive wear in linkage systems.

Further research on railway trains has revealed that while various vehicle parameters generally remain within reasonable ranges during stable operation, a series of issues often arise during train start-up and braking phases. Zhang et al. [28] established a dynamic stability model for the vehicle-locomotive combination, investigating the significant impact of braking force distribution on axle load transfer under braking conditions. Lai et al. [29] developed a three-dimensional dynamic interaction model between freight cars and tracks (switches), which not only simulated longitudinal collisions between cars but also modeled wheel-based braking by vehicle retarders. Comparative analysis of simulation results with derailment field observations revealed that when the front car passes through a retarder section, the longitudinal impact from the rear car significantly increases derailment risk. Zhang et al. [30] established a circulating air-braking model for 20,000-ton heavy-haul train combinations and conducted simulations under downhill braking conditions. The results showed that asymmetric forces between front and rear vehicles during brake release could intensify longitudinal forces. Comparative analysis of these simulation results highlighted the influence of differentiated collaborative control strategies on the longitudinal dynamics of heavy-haul train combinations. Correa et al. [31] utilized Simpack software to develop a 62-degree-of-freedom multibody model for heavy-haul train simulations, conducting experimental studies on applying different abnormal braking forces during straight-line and curve operations.

As can be seen from previous studies, it is evident that most existing studies on railway axle load transfer predominantly employ constant-force traction braking systems. However, actual locomotive braking forces are generated based on electric locomotive motor characteristics. Therefore, variable-force traction braking proves to be a more practical solution. To better understand realistic axle load transfer patterns, this study integrates actual traction braking curves into dynamic models and investigates the impact of different train formations on axle load distribution. Additionally, three distinct axle load transfer improvement strategies are proposed, with corresponding simulation studies and comparative analyses of results conducted.

2. Longitudinal Dynamics Modeling of Vehicles

2.1 Longitudinal Dynamics of Vehicles

Generally, the longitudinal impulse index of a train primarily manifests as longitudinal forces between individual cars and the longitudinal acceleration of vehicles. Train longitudinal dynamics is the scientific study of longitudinal impulses in multi-car formations under operational conditions such as traction, normal braking, and emergency braking. Research by domestic and international experts indicates that factors influencing train longitudinal dynamic performance are highly complex. Among these, the axle load transfer issue-focusing on in this study-is caused by the application of locomotive traction or braking forces. Therefore, it is imperative to establish a train longitudinal dynamics model based on the specific structure of the train.

The railway mode of the semi-trailer used in both public and railway transportation calculated and analyzed in this paper generally includes semi-trailer vehicles, intermediate joint bogies, end conversion bogies and other components, as shown in Fig.1.

ISSN: 2414-1895 DOI: 10.6919/ICJE.202606_12(6).0010

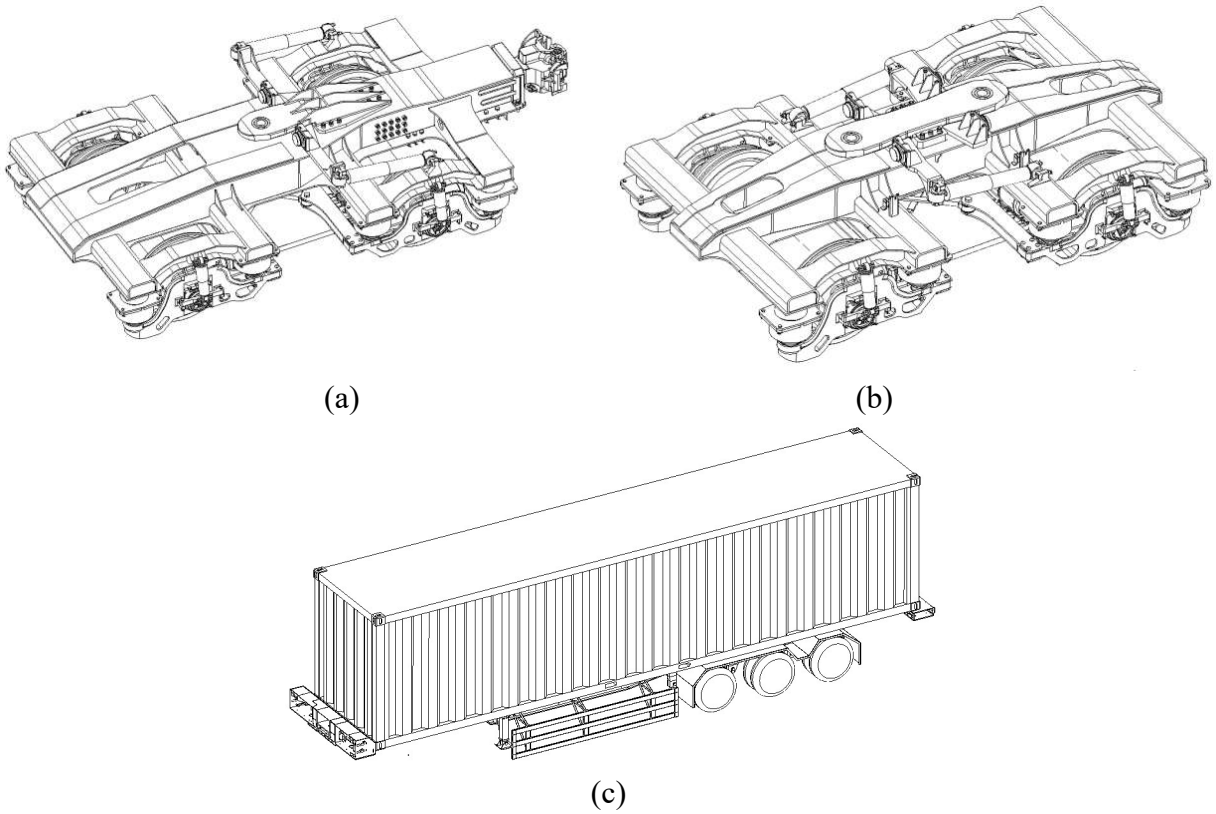

Fig. 1 Body and bogie of a certain type of road-rail vehicle: **a** Transition unit/bogie with coupler device, **b** Intermediate unit/bogie, **c** Car body

As shown in the diagram, vehicles are typically composed of internationally standardized containers and a chassis. The chassis is constructed from welded box-shaped beams and contains road operation mechanisms. The intermediate bogie features symmetrical longitudinal and transverse structures, with its frame made of welded box-shaped beams. It incorporates auxiliary frames, anti-roll dampers, vertical dampers, and longitudinal rubber stops. This bogie is designed for connecting semi-trailer vehicles within various train formations. The end bogie, which is heavier in weight, also uses welded box-shaped beams for its frame. In addition to joint bogie components, it includes coupler buffers and other structural elements. This bogie is specifically designed for connecting train formations as well as linking locomotives with these formations.

In this paper's train longitudinal dynamics simulation model (dynamic schematic diagram as shown in Fig.2:

(1) Simplify the locomotive into a homogeneous rigid body with only longitudinal degrees of freedom.

(2) The longitudinal traction force and braking force of the combined road and rail semi-trailer are transferred between the group units and between the vehicle and the locomotive through the coupler buffer system, and the traction pin between the bogie and the car body is transferred within the group unit.

(3) Because the structure stiffness of vehicles and locomotives is very large, the components such as vehicles and locomotives in the system are usually regarded as homogeneous rigid bodies, and the mass and center of gravity of these components remain unchanged.

(4) The vehicle coupler buffer system is simplified into a spring and damping combined action system according to its characteristics.

(5) No track excitation.

ISSN: 2414-1895 DOI: 10.6919/ICJE.202606_12(6).0010

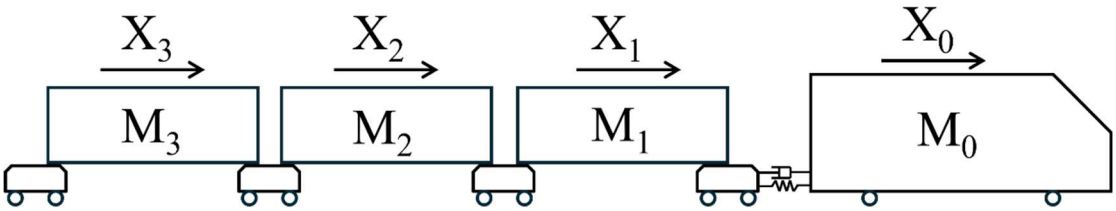

Fig. 2 Schematic diagram of longitudinal dynamic model for road-rail vehicles

2.2 Establishment of Locomotive Model

This section establishes a simplified longitudinal dynamic model for HXD3 electric locomotives based on their specific parameters and modeling assumptions. As a high-power locomotive with a 140-ton standard weight and 1.5-meter center of gravity height, the model treats all components as homogeneous rigid bodies without considering interactions between bogies and other parts. To simulate longitudinal dynamic performance, the model simulates traction force, braking force, and running resistance through their magnitude, position, and duration. The simplified model treats the locomotive as a homogeneous rigid body with only longitudinal degrees of freedom. Since longitudinal force application positions have no effect on mechanical characteristics, all longitudinal forces are applied at the center of gravity. In SIMPACK software, the combination of Hinge 07 and Force Element 51 enables precise force/torque loading through equations. This study employs these force elements to apply traction and braking forces to the model[33].

2.3 Semi-trailer Model Establishment Establishment

The semi-trailer consists of two components: a standard container and a semi-trailer body. The vehicle's fixed wheelbase measures 12,617mm. When empty, the vehicle weighs 6.1t, while under heavy load, the combined weight of the body and container reaches 36t. The vehicle's center of gravity is 2356.5mm above the rail surface. The process of establishing a semi-trailer model in SIMPACK software is largely similar to that of locomotive modeling. During the semi-trailer model construction, longitudinal dynamic modeling assumptions are applied, disregarding interactions between the container and the body, treating them as a single homogeneous rigid body.

2.4 Establishment of the Steering Frame Model

As previously mentioned, the bogies of articulated rail-road dual-purpose freight cars are categorized into two types: intermediate articulated bogies and end conversion bogies. These two bogie types differ in their prepared weight, moment of inertia, and center of gravity positions. The moment of inertia of the bogie is calculated by summing the moments of inertia from major components such as the bogie frame, wheelset, and axle box, while the moments of inertia from smaller components are negligible. Detailed parameters are listed in Table 1.

Table 1. Modeling parameters of the bogie longitudinal dynamic model

Parameter	Intermediate joint bogie	End conversion bogie
Kerb Weight (kg)	6800	8100
Moment of inertia about the X-axis (kg·m²)	2136.28	7793.28
Moment of inertia about the Y-axis (kg·m²)	3103.86	1471.32
Moment of inertia about the Z-axis (kg·m²)	4877.64	8616.64
Height of Bogie Load-Bearing Surface above Rail Top (mm)	1100	1100
Height of Bogie Center of Gravity above Rail Top (mm)	965	963
Wheelbase (mm)	2300	2300

ISSN: 2414-1895 DOI: 10.6919/ICJE.202606_12(6).0010

2.5 Locomotive Traction Characteristics

China is a vast country with a complex geographical environment. When operating on steep gradients, trains encounter substantial slope resistance. To ensure safe operation under complex railway conditions, high-power freight electric locomotives are required to meet design specifications. In accordance with the Railway Industry Standard of the People's Republic of China TB/T 1407.1-2018[32], the HXD3 electric locomotive is selected as the traction engine for the rail-road dual-purpose freight car, as shown in Fig.3.

Fig. 3 HXD3 electric locomotive

This type of locomotive is developed for the development of heavy freight railway transportation in China. The maximum single locomotive can pull 5000t, and the maximum locomotive can pull 20000t.

According to the Railway Industry Standard of the People's Republic of China [3], the traction characteristics of HXD3 locomotive can be approximated as a function of its operating speed, as shown in Equation (1).

$$F = f(v) = \begin{cases} 570 & 0 \le v \le 10 \\ 600.9 - 3.09v & 10 < v \le 65 \\ 26000 / v & 65 < v \le 120 \end{cases} \quad (1)$$

where F -- Wheel-to-track traction force of the locomotive, kN.

v -- Operating speed of the locomotive, km/h.

The traction force and speed-dependent constraint curves of the HXD3 electric locomotive are shown in Fig.4.

(1) When the HXD3 electric locomotive operates at speeds between 0 and 10 km/h, the locomotive limits the maximum starting current. The wheel-circumferential traction force remains constant regardless of operating speed, while the output traction force correlates positively with the driver's lever position. The maximum starting traction force reaches 570 kN.

(2) When the HXD3 electric locomotive operates at speeds ranging from 10 km/h to 65 km/h, the wheel-circumferential tractive force decreases linearly with speed due to the influence of the adhesion coefficient's velocity-dependent variation and the maximum traction power limitation. The specific value follows the second segment of the function f(v).

(3) When the HXD3 electric locomotive operates at speeds between 65km/h and 120km/h, the power limit prevents the traction motor current from increasing continuously. Consequently, the wheel-circumference traction force decreases inversely with speed, with specific values following the third segment of the function f(v).

ISSN: 2414-1895 DOI: 10.6919/ICJE.202606_12(6).0010

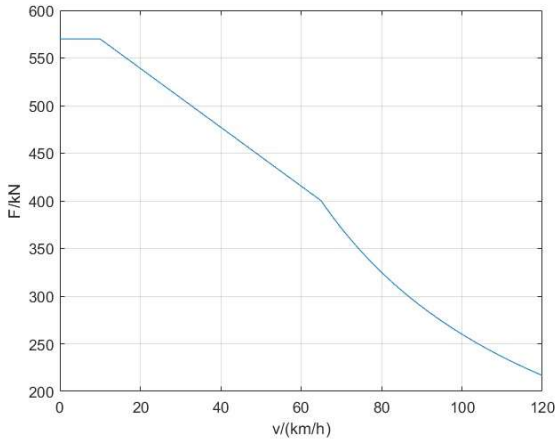

Fig. 4 HXD3-type electric locomotive traction limit curve

2.6 Locomotive Braking Characteristics

The braking force of the articulated rail and road dual-purpose truck can be divided into locomotive braking force and vehicle braking force according to the position of the braking force. The air braking device is installed on both the vehicle and the locomotive, while the power braking device is only installed on the locomotive.

This paper mainly studies the axle load transfer of train under the actual traction brake curve. Through comparative experiments, it is found that the air brake has almost no influence on the axle load transfer, so the air brake is ignored here, and only the influence of power brake on the axle load transfer is studied.

According to the Railway Industry Standard of the People's Republic of China TB/T 1407.1-2018 [32], the locomotive power braking characteristic curve can be approximated as a three-segment function of the locomotive running speed, as shown in Equation (2).

$$F = f(v) = \begin{cases} 36.4\text{-}145.6v & 4 \le v \le 15 \\ 400 & 15 < v \le 65 \\ 26000 / v & 65 < v \le 120 \end{cases} \tag{2}$$

where F-- Wheel-to-track traction force of the locomotive, kN.

v — Operating speed of the locomotive, km/h.

The speed-dependent braking force curve of HXD3 electric locomotive is shown in Fig.5.

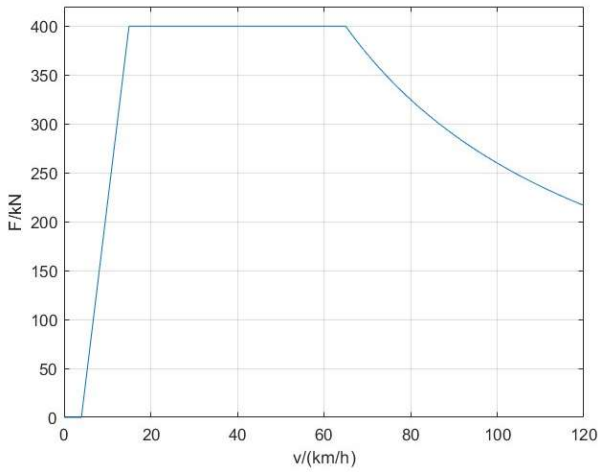

Fig. 5 HXD3-type electric locomotive braking limit curve

ISSN: 2414-1895 DOI: 10.6919/ICJE.202606_12(6).0010

2.7 Coupling Buffer Characteristics

Vehicle connections are typically modeled as integrated traction devices or buffer systems that simulate coupled linkage mechanisms [32]. Electric locomotives are connected to end bogies through couplers and buffers. The longitudinal dynamic performance of trains is directly related to the selection of couplers and buffers. Different coupler types correspond to varying coupler clearances, which determine the speed difference between adjacent train cars and consequently the magnitude of longitudinal impulses. Coupler clearances require precise control during cargo train uncoupling operations and significantly impact smooth train startup. Buffers, as the primary energy-absorbing components, exhibit distinct energy absorption characteristics across different types, substantially affecting longitudinal forces in trains. Selecting appropriate coupler models and longitudinal buffers is a critical step in mitigating train longitudinal impulses.

The freight train currently employs three types of couplers: Series 13, Type 16, and Type 17. Buffer systems are typically categorized into all-steel friction buffers and elastic rubber buffers. The characteristic curve of a buffer illustrates the relationship between resistance and travel distance, which is generally determined through track tests and drop hammer tests. This curve typically comprises two components: the loading curve and unloading curve. The buffer characteristic curve of the coupler used in this study is shown in Fig.6 [4].

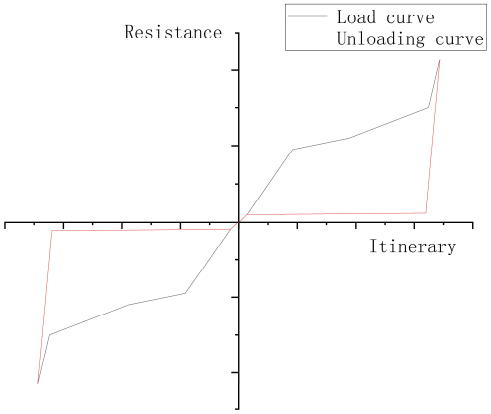

Fig. 6 Buffer characteristic curve diagram

Based on the above analysis, the longitudinal dynamic model of the train in the Simpack software is shown in Fig.7.

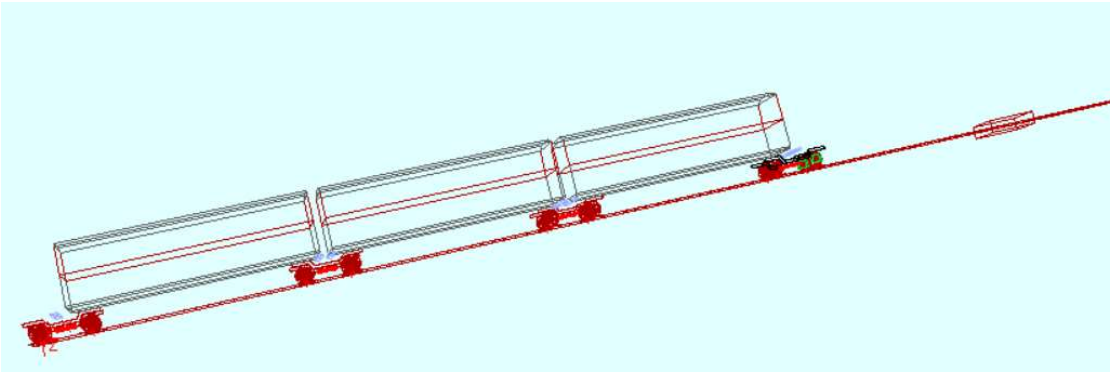

Fig. 7 Longitudinal dynamic model of the train in Simpack software

ISSN: 2414-1895 DOI: 10.6919/ICJE.202606_12(6).0010

3. Simulation and Experimental Comparison

This study investigates a three-section semi-trailer model, simulating axle load transfer during actual traction braking under different configurations: empty carriage(6100 kg, hereafter referred to as “E”) and fully loaded carriage(36000 kg, hereafter referred to as “L”). The formation configurations are as follows: E-E-E, L-E-E, E-E-L, L-E-L, L-L-L.

3.1 Traction Conditions

As shown in Fig.8, there is an obvious impact at the moment of locomotive start-up, and the axle weight of one wheelset decreases suddenly. About 2s later, the axle weight tends to be stable. During the train running, the axle weight still has a trend of slow recovery. When the locomotive reaches the specified speed and the traction force is constant, the axle weight also recovers to the static axle weight.

As shown in Fig.9, there is an obvious impact at the moment of locomotive start-up, which makes the axle weight of the two-wheel pair suddenly increase. About 2s later, the axle weight tends to be stable. During the train running, the axle weight still has a trend of slow recovery. When the locomotive reaches the specified speed and the traction force is constant, the axle weight also recovers to the static axle weight.

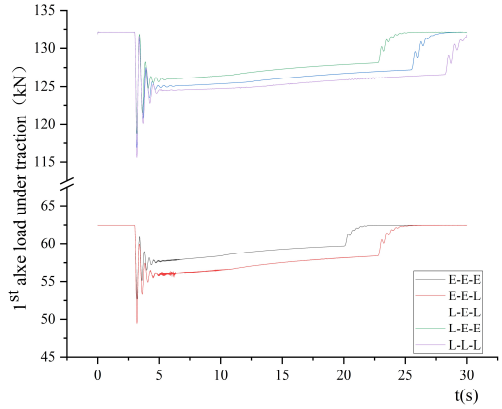

Fig. 8 1st axle load under traction condition

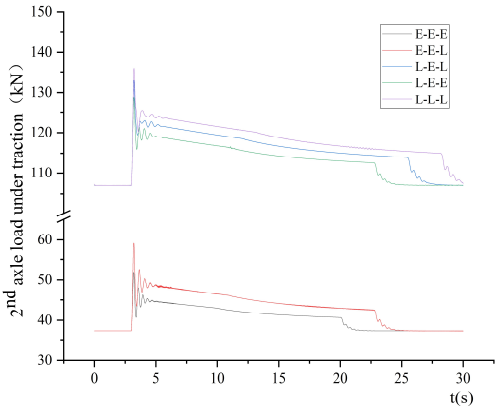

Fig. 9 2nd axle load under traction condition

It can be seen from the above figures that the axle load transfer during impact is significantly higher than that under steady-state conditions. The heavier the total weight of the marshalling train, the greater the magnitude of axle load increase or decrease during impact. Moreover, since a heavier train requires a longer time to accelerate and decelerate, the time needed for axle load recovery is correspondingly prolonged.

3.2 Braking Conditions

As shown in Fig.10, during the train braking process, a significant impact occurs that temporarily increases the axle load of one wheelset. This load quickly stabilizes. As braking force intensifies, the axle load of the affected wheelset gradually rises until reaching its maximum value when the braking force peaks. When the train decelerates to 15 km/h, the braking force begins to diminish, allowing the axle load to gradually recover. Once the train's speed drops to zero, the braking force ceases entirely, and the axle load returns to its static equilibrium state.

As shown in Fig.11, during the train braking process, a significant impact occurs that temporarily reduces the axle load of the second wheelset. This load quickly stabilizes. As braking force increases, the axle load of the second wheelset gradually decreases until reaching its minimum value when maximum braking force is applied. When the train decelerates to 15 km/h, the braking force begins to diminish, allowing the axle load of the second wheelset to recover. Once the speed drops to zero, the braking force ceases, and the axle load returns to its static equilibrium. Simulation results clearly

ISSN: 2414-1895 DOI: 10.6919/ICJE.202606_12(6).0010

demonstrate that when the tail car is heavily loaded, the axle load fluctuation is significantly more pronounced compared to when the tail car is empty.

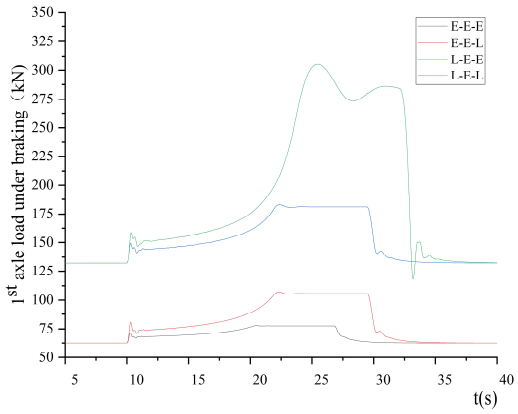

Fig. 10 1st axle load under braking condition

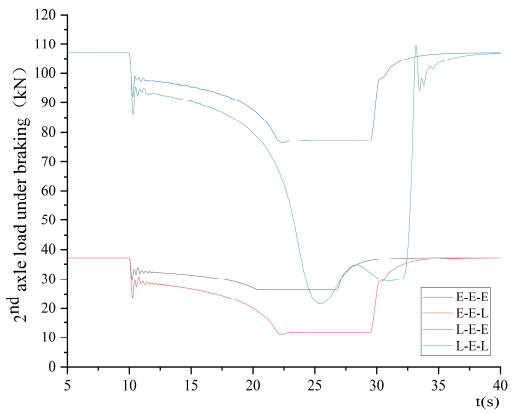

Fig. 11 2nd axle load under braking condition

3.3 Static Tensile and Compression Test

As shown in the Fig.12, the wheelset closest to the derail hook is designated as the 1st wheelset, followed sequentially by the 2nd, 3rd, and 4th wheelsets. The derail hook is positioned at the far right, applying tensile/compressive loads ranging from 100 to 1000kN (with a step size of 100 kN). The tensile load simulates actual traction conditions during operation, while the compressive load corresponds to simulated braking conditions.

Fig. 12 Hook-end bogie schematic

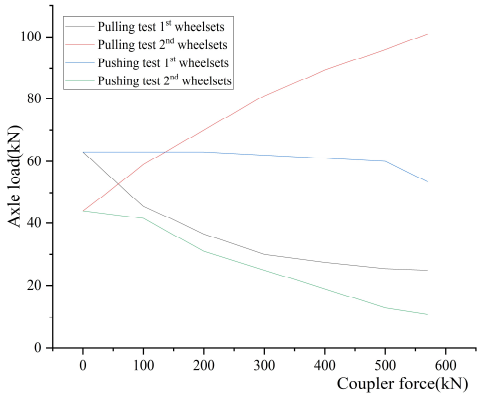

Fig. 13 Results of test

As shown in the experimental data graph in Fig.13, when the coupler force reaches 300–350 kN, the axle load of both the first and second wheel sets has already decreased to 50% of the static axle load. Furthermore, as the coupler force continues to increase, the axle load continues to decrease. Notably, the axle load of the second wheel set has dropped to 10 kN when the coupler force reaches 550 kN, posing a significant derailment risk.

4. Improvement Solutions

4.1 Lower Traction/Braking Position

As shown in Fig.14, lowering the coupler pin height from 1.1m to 0.88m aligns it with the coupler height. This adjustment ensures the traction force on the end bogie and the reaction force from the coupler pin remain at the same horizontal level, eliminating the torque caused by the height difference and thereby resolving the axle load transfer issue.

ISSN: 2414-1895 DOI: 10.6919/ICJE.202606_12(6).0010

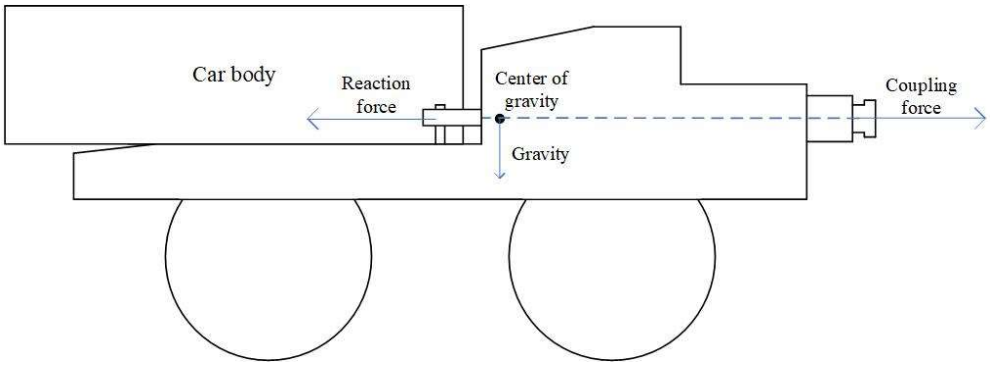

Fig. 14 Schematic diagram of lower traction/braking position

The simulation results are as follows:

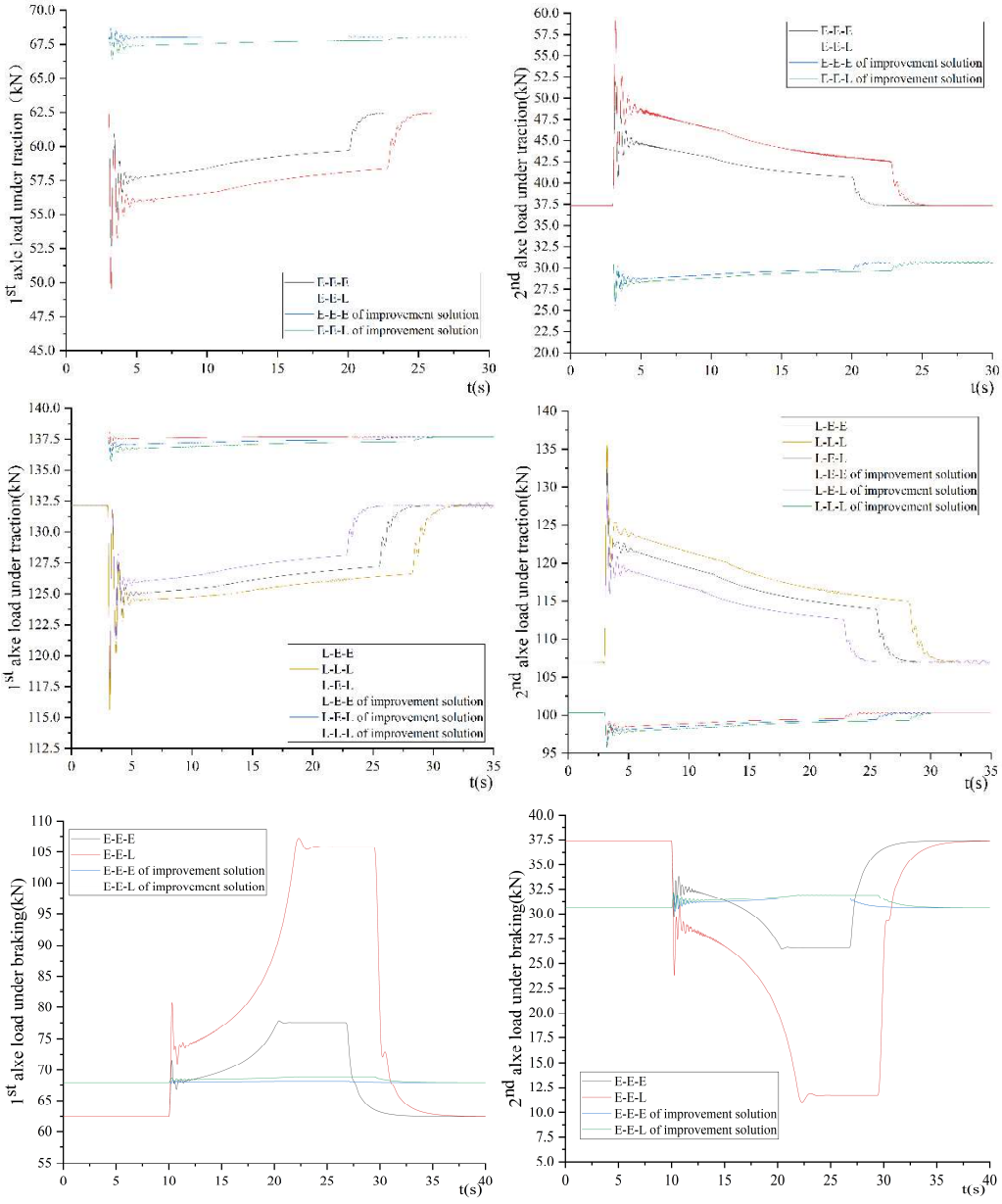

ISSN: 2414-1895 DOI: 10.6919/ICJE.202606_12(6).0010

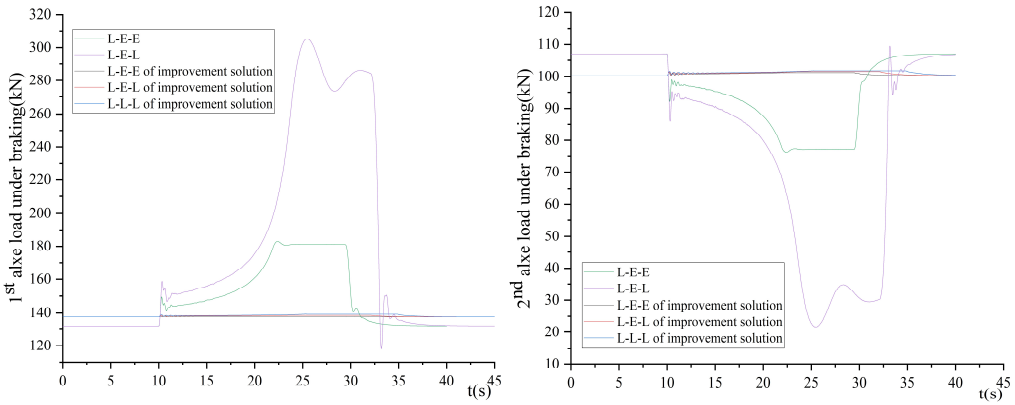

Fig. 15 The comparison of simulation results of original solution and lower traction/braking position

According to the simulation results in Fig.15, the data of the first and second wheel axle weight change of the original scheme and the improved scheme are extracted respectively, and the following table is generated.

Table 2. Axle load variations (kN) under lower traction/braking position of the first wheelset

Traction/Brake conditions	Impact of the original design	Impact of the improvement plan	Steady state of the original design	Steady state of the improvement plan
E-E-E	-9.8/9.1	0.7/0.5	-4.7/15.1	0.1/0.2
E-E-L	-13/18.3	-1.5/0.7	-6.7/43.3	-0.6/0.9
L-E-E	-13.3/17.3	-1.2/0.2	-5.9/48.9	-0.6/0.2
L-E-L	-15.1/26.5	-1.4/0.7	-7/144.5	-0.6/0.9
L-L-L	-16.5/ -	-1.8/1.3	-7.7/ -	-0.9/1.6

Table 3. Axle load variations (kN) under lower traction/braking position of the second wheelset

Traction/Brake conditions	Impact of the original design	Impact of the improvement plan	Steady state of the original design	Steady state of the improvement plan
E-E-E	14.6/-7.6	-4.6/1.5	7.2/-10.7	-2.4/1.0
E-E-L	21.8/-13.6	-5/1.6	11.3/-25.6	-2.3/1.3
L-E-E	21.7/-14.9	-3.9/1.1	12.1/-29.8	-1.7/0.9
L-E-L	25.8/-21	-4.2/1.2	14.6/-77.5	-2.1/1.2
L-L-L	28.9/ -	-4.5/1.4	16.5/ -	-2.3/1.5

The comparison in the chart above reveals that adjusting the vehicle's sales height resulted in a 6kN increase in static axle load for one wheelset and a 6kN decrease for the other. Both wheelsets showed significant improvements in axle load performance during impact and stable conditions, with loads consistently maintained below 2kN. This effectively resolved the axle load transfer issue.

4.2 Mounting the Coupling on the Car Body

The original coupler is discarded and a new type of coupler is installed on the car body, as shown in Fig.16. The force couple is eliminated by changing the position of the force, so as to improve the problem of axle weight transfer.

ISSN: 2414-1895 DOI: 10.6919/ICJE.202606_12(6).0010

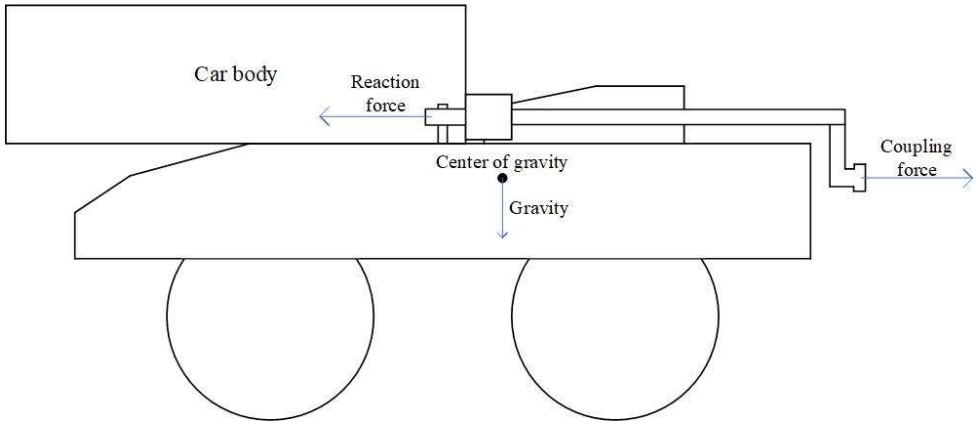

Fig. 16 Schematic diagram of the coupler placed on the car body

The simulation results are as follows:

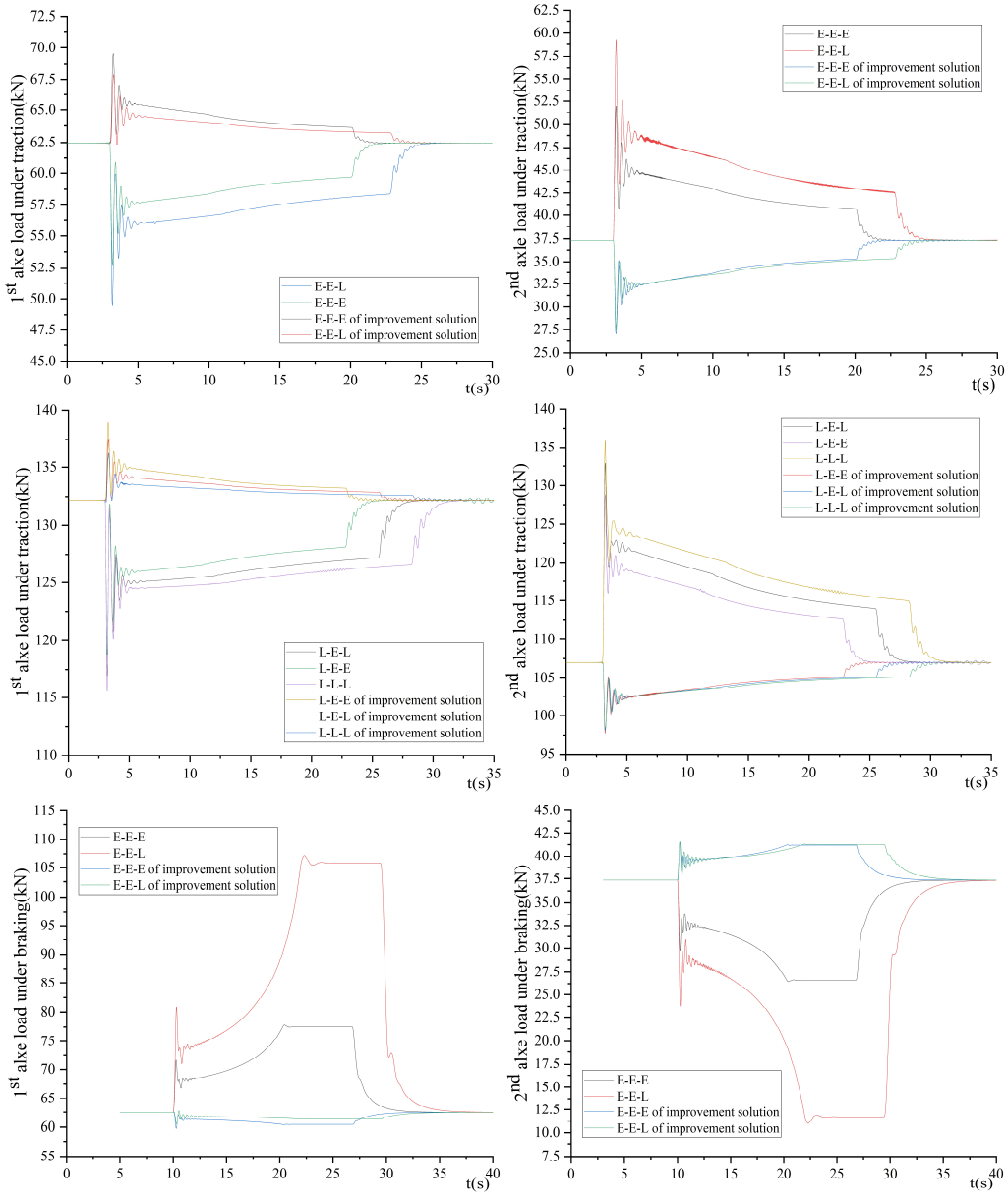

ISSN: 2414-1895 DOI: 10.6919/ICJE.202606_12(6).0010

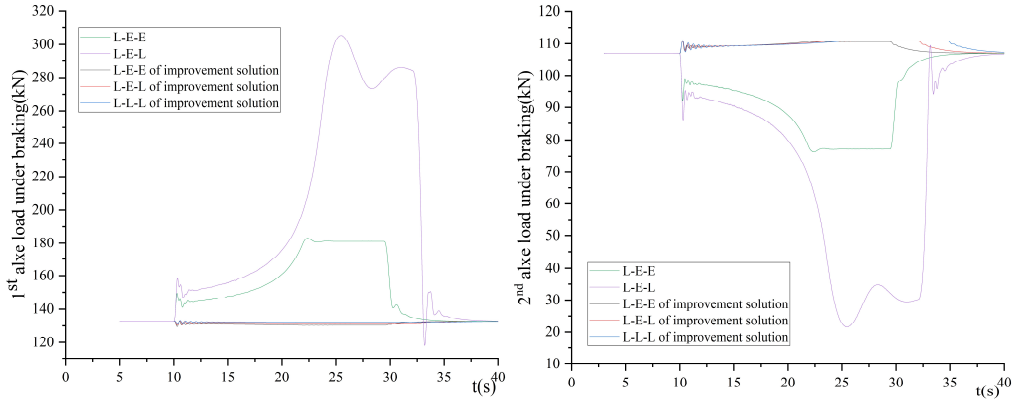

Fig. 17 The comparison of simulation results of original solution and mounting the coupling on the car body

According to the simulation results in Fig.17, the data of the first and second wheel axle weight change of the original scheme and the improved scheme are extracted respectively, and the following table is generated.

Table 4. Axle load variations (kN) under mounting the coupling on the car body of the first wheelset

Traction/Brake conditions	Impact of the original design	Impact of the improvement plan	Steady state of the original design	Steady state of the improvement plan
E-E-E	-9.8/9.1	7.1/-2.7	-4.7/15.1	2.9/-2.0
E-E-L	-13/18.3	5.4/-1.9	-6.7/43.3	2.1/-1.1
L-E-E	-13.3/17.3	6.8/-2.6	-5.9/48.9	2.9/-1.8
L-E-L	-15.1/26.5	5.3/-1.8	-7/144.5	1.9/-1.1
L-L-L	-16.5/ -	4.1/-1.2	-7.7/ -	1.4/-0.5

Table 5. Axle loadvariations (kN) under mounting the coupling on the car body of the second wheelset

Traction/Brake conditions	Impact of the original design	Impact of the improvement plan	Steady state of the original design	Steady state of the improvement plan
E-E-E	14.6/-7.6	-10.3/4.2	7.2/-10.7	-5.0/3.8
E-E-L	21.8/-13.6	-10.0/4.2	11.3/-25.6	-5.0/3.9
L-E-E	21.7/-14.9	-9.3/3.8	12.1/-29.8	-4.7/3.6
L-E-L	25.8/-21	-8.9/3.9	14.6/-77.5	-4.5/3.7
L-L-L	28.9/ -	-8.7/4.0	16.5/ -	-4.4/3.8

As can be seen from the chart, due to the change of the position of the coul, the position of the force acting changes successively, resulting in the increase and decrease of the axle weight in the opposite direction to the original scheme; at the same time, the axle weight of the first and second wheel sets has been greatly improved, and both are controlled at about 4kN.

ISSN: 2414-1895 DOI: 10.6919/ICJE.202606_12(6).0010

4.3 Drawing on the U.S. Rail-runner Program

Adopting the American model with optimized adaptations, the load-bearing points of the end bogies are shifted 0.3 meters toward the second wheelset while being elevated 3mm. The pin positions are moved 0.8 meters toward the first wheelset from the center between the first and second wheelsets. The pins of the intermediate bogie connected to Car No.1 are raised to a bypass height of 1.24 meters above ground level, resulting in Car No.1 maintaining a minimal tilt angle as shown in Fig.18. Due to the force distribution shift toward the second wheelset, the train's static axle load theoretically transfers from the first to the second wheelset, thereby optimizing the load distribution to address axle load transfer issues.

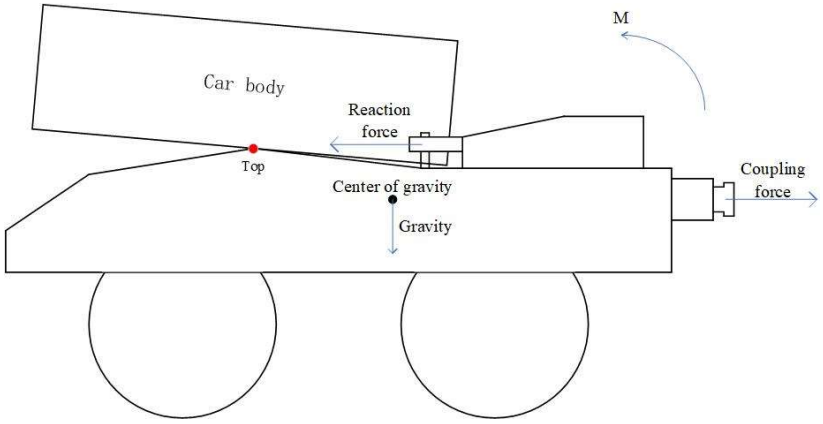

Fig. 18 Schematic diagram of improved the U.S. Railrunner program

The simulation results are as follows:

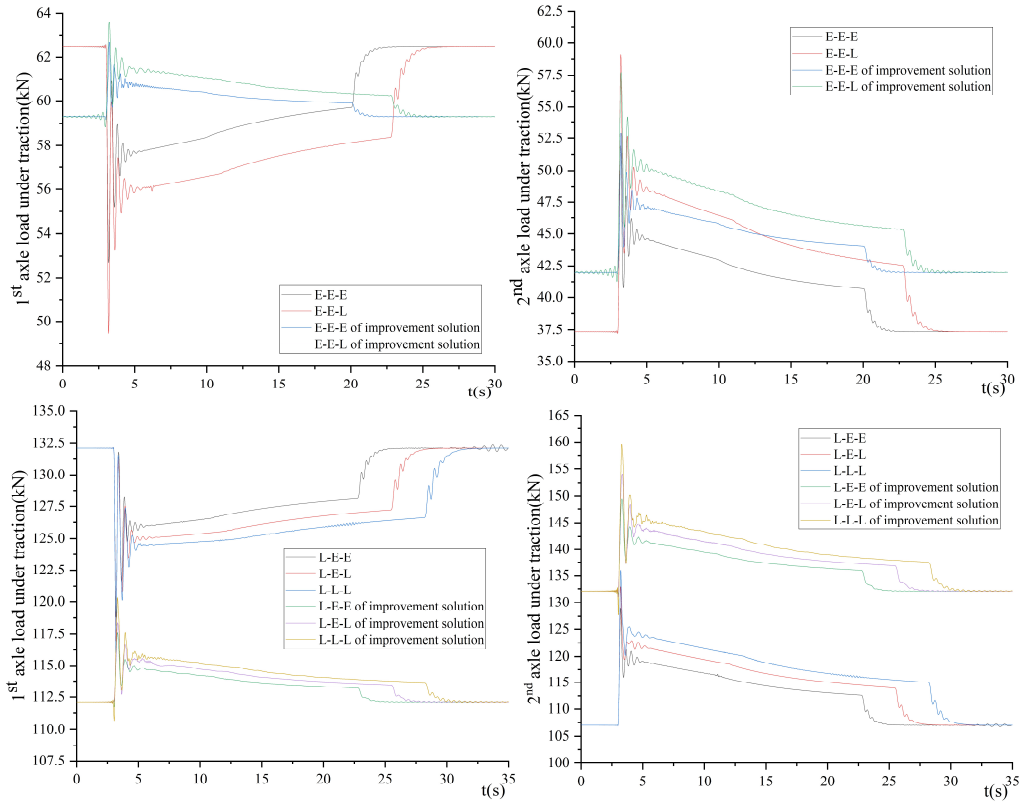

ISSN: 2414-1895 DOI: 10.6919/ICJE.202606_12(6).0010

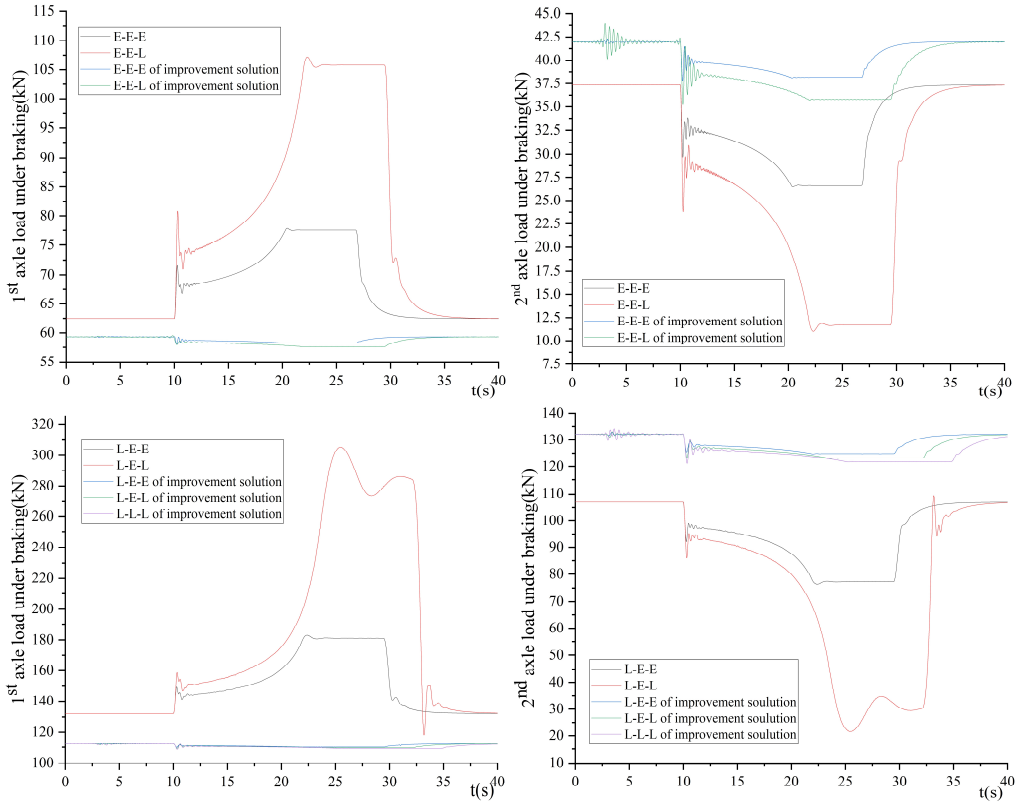

Fig. 19 The comparison of simulation results of original solution and drawing on the U.S. Rail-runner program

According to the simulation results in Fig.19, the data of the first and second wheel axle weight change of the original scheme and the improved scheme are extracted respectively, and the following table is generated.

Table 6. Axle load variations (kN) under improved the U.S. Rail-runner program of the first wheelset

Traction/Brake conditions	Impact of the original design	Impact of the improvement plan	Steady state of the original design	Steady state of the improvement plan
E-E-E	-9.8/9.1	3.4/-1.4	-4.7/15.1	1.4/-1.1
E-E-L	-13/18.3	4.3/-2.7	-6.7/43.3	2.0/-1.7
L-E-E	-13.3/17.3	5.5/-2.2	-5.9/48.9	2.5/-2.1
L-E-L	-15.1/26.5	6.3/-2.9	-7/144.5	3.0/-2.5
L-L-L	-16.5/ -	8.2/-3.5	-7.7/ -	3.4/-0.9

Table 7. Axle load variations (kN) under improved the U.S. Railrunner program of the second wheelset

Traction/Brake conditions	Impact of the original design	Impact of the improvement plan	Steady state of the original design	Steady state of the improvement plan
E-E-E	14.6/-7.6	11.0/-4.2	7.2/-10.7	4.9/-3.8
E-E-L	21.8/-13.6	15.7/-6.8	11.3/-25.6	7.9/-6.2
L-E-E	21.7/-14.9	17.4/-6.7	12.1/-29.8	9.1/-7.3
L-E-L	25.8/-21	21.9/-8.9	14.6/-77.5	11.3/-9.0
L-L-L	28.9/ -	27.5/-10.9	16.5/ -	13.1/-10.3

ISSN: 2414-1895 DOI: 10.6919/ICJE.202606_12(6).0010

The original design suffered from uneven static axle load distribution between the first and second wheelsets due to traditional bogie structure limitations, resulting in significantly poorer performance of the second wheelset's axle load distribution compared to the first. Analysis of charts reveals that during empty train operation, approximately 5kN of static axle load shifts from the first to the second wheelset, while heavy-load conditions see this transfer increase to about 20kN. This redistribution effectively mitigates axle load risks in the second wheelset. Additionally, minor improvements have been achieved in axle load transfer during impact and stability scenarios. The combined application of these two aspects demonstrates enhanced axle load transfer optimization.

5. Summary

This study applies actual traction braking curves to train dynamics models, simulating different train formations through combinations of empty and fully loaded carriage. The research investigates how varying formation configurations affect axle load transfer, revealing the following findings: When the total weight of a formation train is substantial, both impact and stable conditions exhibit greater axle load transfer values. Moreover, increased vehicle weight prolongs acceleration/deceleration times, extends the duration of traction braking application, and consequently delays axle load recovery. These observations suggest that long formation trains and heavy-haul trains experience more severe and prolonged axle load transfer issues during traction braking processes.

Through analysis of axle load transfer issues, we identify that the root cause stems from rotational moments generated when coupler forces and pin reaction forces operate at different elevations. Furthermore, China's traditional end bogies exhibit a pronounced weight distribution bias toward the first wheelset, while the coupler system itself carries substantial weight. This results in the first wheelset bearing significantly heavier static axle loads than the second wheelset. Consequently, load reduction measures on the second wheelset are more prone to derailment risks. Based on this analysis, the study proposes three optimized solutions for axle load transfer mitigation. Through comprehensive simulation evaluations, we systematically examine load distribution patterns under each configuration and conduct comparative analyses with baseline designs, ultimately deriving the following conclusions:

Lower traction/brake position: This solution eliminates the height difference between the coupler force and the reaction force of the coupler pin, thereby removing the rotational torque. Simulation results show that both during impact and stable conditions, the axle load variation in single-and double-vehicle wheelsets remains within 2kN, effectively resolving axle load transfer issues.Simplify the locomotive into a homogeneous rigid body with only longitudinal degrees of freedom.

Mounting the coupling on the car body: By adjusting the coupler's position to modify the force application point, the rotational torque is eliminated. Simulation results indicate that the weight distribution patterns of the first and second axle positions are reversed compared to the original design. Furthermore, the axle weight variations in both wheelsets are maintained at approximately 4kN, effectively resolving the axle weight transfer issue.

Drawing on the U.S. Railrunner program: This solution adjusts the horizontal alignment between vehicle sales and bypass channels by modifying the load-bearing points of the vehicle body to balance the static axle loads between the first and second wheelsets. Simulation results indicate that under empty conditions, the static axle load shifts approximately 5kN from the first wheelset to the second. Under heavy load conditions, this transfer increases to about 20kN. Additionally, the system demonstrates minor improvements in axle load variations during impact and stable conditions. The combination of these two methods effectively addresses axle load transfer issues.

References

[1] Jason, M., & Bergqvist, R. (2017). *Intermodal freight transport and logistics*. CRC Press.

[2] Anonymous. (2016). Transnet adopts RailRunner intermodal system. *International Railway Journal*, 56(10).

ISSN: 2414-1895 DOI: 10.6919/ICJE.202606_12(6).0010

[3] Anonymous. (2006). Bogies for RailRunner. *Traffic World*, 270(25), 32.

[4] Anonymous. (2014). Low-emission Unimog on show. *Railway Gazette International*, 170(9), 154.

[5] Anonymous. (2010). Road-rail tunnel. *Railway Gazette International*, 166(9).

[6] Li, Z. H., Li, F., & Li, C. X. (2019). Status and development of road-rail vehicles in urban rail transit. *Electric Locomotive & Mass Transit Vehicle*, 42(1), 1–5. (in Chinese)

[7] Zhao, Z. N., Xu, N., & Li, H. T. (2018). Analysis of the development status and trends of road-rail vehicles at home and abroad. *Special Purpose Vehicle*, (7), 33–37. (in Chinese)

[8] Dong, H., Chen, J. J., Zhu, J., et al. (2023). Overview of research and application of road-rail vehicles. *Railway Vehicle*, 61(3), 39–48. (in Chinese)

[9] Wang, J. C., Ling, L., Chen, Z., Wang, K. Y., & Zhai, W. M. (2025). Nonlinear stability of railway locomotive system subjected to longitudinal in-train force. *Applied Mathematical Modelling*, 143, 116056.

[10] Sun, S. L., Ding, J. J., Zhou, Z. Y., et al. (2017). Dynamic analysis and experimental study on longitudinal impulse of heavy-haul trains. *Journal of Mechanical Engineering*, 53(8), 138–146. (in Chinese)

[11] Schwarz, C., Heckmann, A., & Heckmann, B. (2017). Observability measures for the longitudinal dynamics of railway vehicle bogies. In *Dynamics of Vehicles on Roads and Tracks* (Vol. 2, pp. 1227–1232).

[12] Craciun, C., et al. (2018). Influence of resistance to motion of railway vehicles on the longitudinal trains dynamics. *MATEC Web of Conferences*, 178, 06003. https://doi.org/10.1051/matecconf/201817806003

[13] Wu, Q., Spiryagin, M., et al. (2024). Introducing wheel-rail adhesion control into longitudinal train dynamics. *International Journal of Heavy Vehicle Systems*, 31(3), 289–306.

[14] Magelli, M., Zampieri, et al. (2024). A novel approach for longitudinal train dynamics simulations with multibody codes. *Vehicle System Dynamics*, 1–19.

[15] Wu, P. P., Ding, J. J., Zhang, M. S., et al. (2017). Calculation and analysis of axle load transfer for A-1-A axle arrangement locomotive. *Railway Locomotive & Car*, 37(1), 14–19+112. (in Chinese)

[16] Yang, Y. J. (2007). Influence analysis of gradient on locomotive axle load transfer. *Railway Locomotive & Car*, (2), 7–11. (in Chinese)

[17] Liu, L. Z. (2015). Simulation research on axle load transfer of electric locomotive based on multi-body dynamics. *Journal of Lanzhou Jiaotong University*, 34(4), 137–140. (in Chinese)

[18] Wang, Z. C., Chen, Z. G., Zhai, W. M., et al. (2019). Research on axle load transfer of heavy-haul electric locomotive considering gear transmission system. *Journal of the China Railway Society*, 41(10), 24–29. (in Chinese)

[19] Luo, J. L. (2022). Research on axle load transfer of medium-low speed maglev traction vehicle. *Locomotive & Electric Drive*, (1), 79–84. (in Chinese)

[20] Xuan, T. P., Okuma, M., & Bur, M. (2021). Basic study on weigh-in-motion of vehicles in acceleration and deceleration. *Mechanical Engineering Journal*, 8(1), 1–10.

[21] Wei, L., & Zeng, J. (2022). Longitudinal-vertical dynamics of a high-speed train rescued by locomotives during braking on grades. *Vehicle System Dynamics*, 61(6), 1476–1499. https://doi.org/10.1080/00423114.2021.2025227

[22] Zhang, N., Xiao, H., & Hermann, W. (2016). Nonlinearity-induced time-varying harmonic dynamic axle load and its impact on dynamic stability of car-trailer combinations. *Vehicle System Dynamics*, 54(5–6), 848–870. https://doi.org/10.1080/00423114.2015.1136525

[23] Wu, Q., et al. (2013). Coupler jackknifing and derailments of locomotives on tangent track. *Vehicle System Dynamics*, 51(11), 1784–1800. https://doi.org/10.1080/00423114.2013.815852

[24] Yadav, O. P., & Vyas, N. S. (2023). Influence of slack of automatic AAR couplers on longitudinal dynamics and jerk behaviour of rail vehicles. *Vehicle System Dynamics*, 61(9), 2317–2337. https://doi.org/10.1080/00423114.2022.2164902

[25] Zhang, J., et al. (2023). Collision characteristics of the intermediate coupler of a rail vehicle. *Vehicle System Dynamics*, 61(12), 3089–3110. https://doi.org/10.1080/00423114.2023.2239074

[26] Yang, C., et al. (2022). Calculation method for maximum swing angle in vertical direction of rail vehicle coupler. *Journal of Vibration and Shock*, 41(15), 153–160+216.

ISSN: 2414-1895 DOI: 10.6919/ICJE.202606_12(6).0010

[27] Hu, X., et al. (2024). Research on abnormal wear mechanism of the coupler system in heavy-haul trains. *Vehicle System Dynamics*, 1–29.

[28] Zhang, N., Wu, J. H., & Li, T. (2021). Influence of braking on dynamic stability of car-trailer combinations. *Proceedings of the Institution of Mechanical Engineers, Part D: Journal of Automobile Engineering*, 235(2–3), 455–464. https://doi.org/10.1177/0954407020952478

[29] Lai, J., Xu, J., Chen, Y., et al. (2023). Evaluation of dynamic derailment in a railway switch considering the longitudinal impacts caused by vehicle retarder. *Proceedings of the Institution of Mechanical Engineers, Part F: Journal of Rail and Rapid Transit*, 237(6), 806–817. https://doi.org/10.1177/09544097221148225

[30] Zhang, W., Li, W., Fan, Y., et al. (2024). Influence of cyclic pneumatic brake on the longitudinal dynamics of heavy-haul combined trains. *IEEE Transactions on Intelligent Transportation Systems*, 25(3), 2545–2557. https://doi.org/10.1109/TITS.2023.3327818

[31] Corrêa, P. H. A., Ramos, P. G., Teixeira, L. H. S., et al. (2023). Dynamic simulation of a heavy-haul freight car under abnormal braking application on tangent and curve. *Vehicle System Dynamics*, 61(9), 2456–2471. https://doi.org/10.1080/00423114.2022.2169509

[32] Wu, Q., Spiryagin, M., & Cole, C. (2016). Longitudinal train dynamics: an overview. *Vehicle System Dynamics*, 54(12), 1688–1714. https://doi.org/10.1080/00423114.2016.1230509

[33] National Railway Administration of the People's Republic of China. (2018). *Railway industry standard: TB/T 1407.1-2018*. (in Chinese)